Check for updates

The pH-triggered drug release and simultaneous carrier decomposition of effervescent SiO$_2$–drug–Na$_2$CO$_3$ composite nanoparticles: to improve the antitumor activity of hydrophobic drugs

Tianyu Chen, [iD] Yichun Jiang, Changmao Wang, Zhengxue Cai, Hui Chen, Junliang Zhu, Pinrun Tao and Min Wu [iD] *

To achieve a better release effect of hydrophobic drugs and spontaneous nanocarrier disintegration by dissolution as well as the CO$_2$ production of Na$_2$CO$_3$ further, improving the therapeutic effect of hydrophobic drugs, and thereby avoiding the accumulation of the nanocarrier *in vivo* to produce organ toxicity, effervescent SiO$_2$–drug–Na$_2$CO$_3$ composite nanoparticles (ESNs) were prepared in this study using a tetraethyl orthosilicate hydrolysis method. Sodium carbonate was used as the effervescent disintegrant to respond to the acidic microenvironment of the tumor. The properties of ESNs were assessed and TEM images were taken to verify the self-disintegration characteristics of nanocarrier materials. The *in vitro* anticancer efficacy of ESNs was evaluated in human breast cancer MCF-7 cells. ESNs loaded with hydrophobic drugs were successfully constructed, and showed high entrapment efficiency and drug loading. The nanocarrier successfully achieved self-disintegration in a PBS environment of pH value at 5.0, and showed excellent antitumor effect *in vitro*. ESNs can effectively load hydrophobic drugs and achieve self-disintegration, while avoiding toxicity from the accumulation of the nanocarrier. These results suggest that ESNs are a promising drug delivery system capable of maximizing the anticancer therapeutic efficacy and minimizing the systemic toxicity.

Introduction

The delivery of hydrophobic drugs, especially the combinative but hydrophobic drugs, generally comes as a huge challenge to researchers.[1,2] An ideal nanoparticle (NP) carrier-drug system for these water-insoluble drugs should possess several traits, including effective drug-loading, efficient cellular internalization, controllable but complete release, and thorough elimination from the biological body after its function.[3–5] Despite the modern advances of various forms of drug delivery systems, none of those existing excogitations can simultaneously meet the above four criteria. In particular, the controlled release and carrier self-decomposition into very tiny particles are highly craved, but hardly realized for these poorly soluble drugs.[6]

In recent decades, silica nanoparticles (SNs) have achieved tremendous advances in improving the efficacy of drug delivery in cancer therapeutics.[7,8] SNs possess great biocompatibility, an ordered mesoporous structure, a large specific surface area providing sufficient space for the accommodation of drugs, and easy surface-functional modification for the promotion of cell uptake.[9] They can also be used as controlled drug-delivery vehicles *via* the simple alteration of SNs or mesoporous size.[10]

Generally, three strategies have been employed for the loading of drugs into SiO$_2$ nanocarriers. These strategies include either normally with the chemical molecules reposing in the pores of mesoporous SiO$_2$ NPs (MSN) and being attached on the exterior or interior surface of the NPs, *via* physical adsorption or chemical bonding, or specially being inserted in the dense SiO$_2$ NPs. With drug release, considerable success has been achieved through various mechanisms. Among those, the gated MSN is probably the best known. In the gated MSN, the pores loaded with drug molecules are plugged by a variety of substances that are responsive to either physical or chemical stimuli. Drug release can be realized by exposure of the NPs to fluctuating physical or chemical conditions, such as temperature, light, and pH.[11–13] A distinct method of controlled release can also be obtained *via* forming various pore morphologies. However, when delivering the hydrophobic drugs, the drug loading and controlled release further generating an efficient drug concentration are difficult to gain due to their lack of high concentration gradient. At the same time, due to the stability of the silicon–oxygen bond, the SNs' clearance period *in vivo* is as long as 4 weeks. Most of them still maintain their size and charge, resulting in the accumulation *in vivo*, and contribute to the difficulties in the cargo release in turn.

School of Pharmacy, Chengdu Medical College, No. 783, Xindu Avenue, Xindu District, Chengdu, Sichuan Province, P. R. China. E-mail: wuminzhaofeng@126.com; Tel: +86-28-6230-8653

Some attempts have emerged to promote the disintegration of MSNs in recent years. For example, disulfide bonds are introduced into the silicon–oxygen bonds in response to the tumor-reducing environment, and lead to the partial breakage of the silicon–oxygen bonds. Alternatively, the incorporation of water-soluble drugs into the SiO_2 carrier network gives rise to the drug release, while pulling the disintegration of the MSNs.[14–16] In the latter work, an ingenious NPs was devised that simultaneously featured the controlled release and carrier decomposition using a special type of SiO_2 carrier-drug composite NPs. A structural hallmark of the NP carrier-drug is that the model molecules are mainly concentrated in the NP center. In the meantime, a loose SiO_2 framework is entangled with the model molecules in the NPs. Drug release is primarily stimulated by the dissolution of model molecules and diffusion when exposed in the body fluid. In turn, this triggers the SiO_2 carrier decomposition.[5,17] Obviously, the methodology can only be applied to water-soluble chemical molecules.

Here, taking berberine (BBR) (Fig. 1A) and evodiamine (EVO) (Fig. 1B) as a pair of synergistic and hydrophobic drug examples, we fabricated a composite nano system (ESNs) with a core–shell structure. Inside of the ESNs, the guest drug molecules, as well as sodium carbonate (Na_2CO_3), a gas-generating agent widely used as an alkali source of an effervescent disintegrator when exposed in an acidic environment was highly concentrated in the SNs center. It manifested a radial drug concentration gradient, accompanied with a loose SiO_2 framework entangled with the model molecules in the NPs. Outside of ESNs, a drug-loaded lipid film of DSPE-PEG 2000 was coated on the surface, which can prolong its circulation time, combining the good biocompatibility of SNs and affinity to the tumor cells of liposomes.[18] The nanocarriers with a unique feature in this study enable the pH-triggered controllable and comparatively complete release of the hydrophobic drugs, and the simultaneous carrier decomposition of SNs for easy system excretion driven primarily by CO_2 gas generation (Scheme 1).

Materials and methods

Materials

Berberine (BBR), evodiamine (EVO), coptisine (COP) (Fig. 1C), luteolin (LUT) (Fig. 1D), and cyanidin-3-O-glucoside (C3G) (Fig. 1E) were purchased from Chengdu Pufei De Biotech Co., Ltd (Chengdu, China). Tetraethyl orthosilicate (TEOS) was purchased from Sinopharm Chemical Reagent Co., Ltd (Shanghai, China). DSPE-PEG2000, cholesterol, and hydrogenated lecithin (HSPC) were purchased from Shanghai Yuanye Biotechnology Co., Ltd (Shanghai, China). Sodium carbonate, ammonia, chloroform, and 95% ethanol were purchased from Chengdu Kelong Chemical Reagent Plant (Chengdu, China). Dulbecco's modified Eagle's medium (DMEM), fetal bovine serum (FBS), and phosphate-buffer solution (PBS) were purchased from Gibco (Uxbridge, UK). Hoechst Staining Kit, Annexin V-FITC Apoptosis Detection Kit, trypsin, 3-(4,5-dimethylthiazol-2-yl)-2,5-diphenyltetrazoliumbromide (MTT), and dimethyl sulfoxide (DMSO) were purchased from Sigma-Aldrich (St. Louis, MO). All other reagents were of analytical grade and were used as supplied.

Cell lines and cultures

Human umbilical vein endothelial cells (HUVECs) and HEK-293 human embryonic kidney cells were purchased from Procell Life Science & Technology (Wuhan, China). MCF-7 human breast carcinoma cells were obtained from the Department of Pharmacy, Sichuan University (Chengdu, China). All cell lines
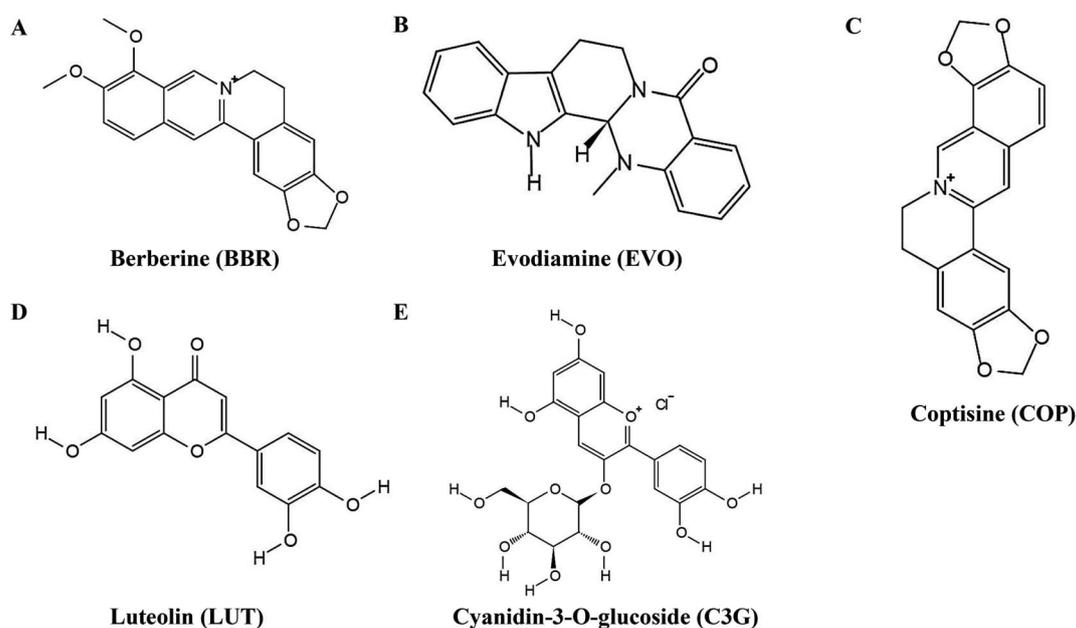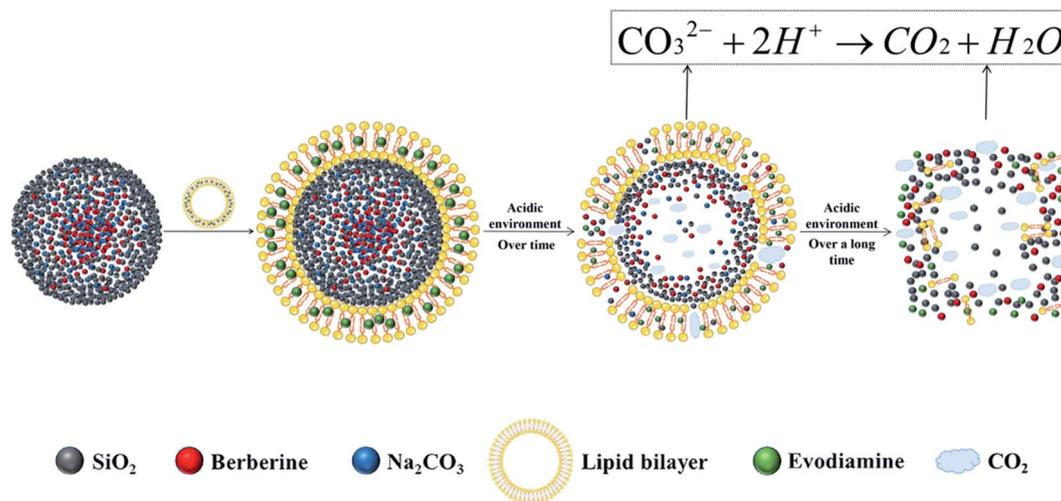

Fig. 1 Chemical structures of (A) berberine, (B) evodiamine, (C) coptisine, (D) luteolin and (E) cyanidin-3-O-glucoside.

$$CO_3{}^{2-} + 2H^+ \rightarrow CO_2 + H_2O$$

SiO₂   Berberine   Na₂CO₃   Lipid bilayer   Evodiamine   CO₂

Scheme 1 Schematic illustration of the make-up of ESNs, pH-triggered drug release and simultaneous carrier decomposition.

were cultured in DMEM with 10% fetal bovine serum, and were incubated at 37 °C in a humidified incubator with 5% CO_2.

Preparation of ESNs

Preparation of SiO₂–BBR–Na₂CO₃. SiO_2–BBR–Na_2CO_3 NPs were prepared using a tetraethyl orthosilicate hydrolysis method.[19] BBR (4 mg) and sodium carbonate (2.5 mg) were dissolved in 30 mL of 95% ethanol. TEOS (0.05 mL) and ammonia (3.4 mL) were added to the solution and reacted at 30 °C under intensive magnetic stirring for 24 h. The mixtures were washed with 95% ethanol and deionized water three times in order to completely remove the residual reactants. The resulting reaction solution was centrifuged for 10 min at 16 000 g in a refrigerated centrifuge. The SiO_2–BBR–Na_2CO_3 NPs were collected by vacuum drying for 24 h.

Preparation of EVO-LB. HSPC (6 mg), cholesterol (2 mg), DSPE-PEG2000 (2 mg) and EVO (5 mg) were dissolved in 5 mL of chloroform in a round-bottomed flask. The organic solvent was removed using rotary evaporation to form the lipid bilayer membrane (EVO-LB).

Preparation of SiO₂–BBR–Na₂CO₃@EVO-LB (ESNs). SiO_2–BBR–Na_2CO_3 (10 mg) NPs were dissolved in 5 mL of deionized water, and sonicated using a probe sonicator at 30 W for 5 min to form the nanoparticle suspension. The suspension was added to the EVO-LB, and further sonicated at 30 W for 30 min in an ice bath. The mixtures were washed with deionized water three times in order to completely remove the residual reactants. The resulting reaction solution was centrifuged for 10 min at 11 000 g in a refrigerated centrifuge. The nanoparticles of SiO_2–BBR–Na_2CO_3@EVO-LB NPs were collected by vacuum drying for 24 h.

NPs of the control groups lacking EVO, BBR or Na_2CO_3 were prepared analogously. All nanoparticles were stored at 4 °C before use.

Characterization of ESNs

Particle size and zeta potential. The average particle size and zeta potential of the ESNs were measured at 25 °C using a Zetasizer Nano ZS 90 (Malvern Instruments, Malvern, UK). Each material was tested in triplicate.

Morphology. The morphology of the ESNs was analyzed by transmission electronic microscopy (TEM). ESNs were diluted with deionized water, placed on a copper grid and stained with 2% (w/v) phosphotungstic acid solution for 30 s.[20] Excess fluid was removed with a piece of filter paper. The sample was then allowed to dry at room temperature, and it was examined on a JEM 1400 microscope (JEOL, Tokyo, Japan).

Entrapment efficiency and drug loading. The entrapment efficiency (EE%) and drug loading (DL%) of EVO and BBR in ESNs were determined using high-performance liquid chromatography (HPLC; Agilent Technologies, Santa Clara, CA, USA). The sodium carbonate content (Na_2CO_3%) in ESNs was determined using acid–base titration method. The EE%, DL% of the drug and Na_2CO_3% were calculated using the following formulas:

$$EE\% = \frac{\text{weight of drug in nanoparticles}}{\text{weight of drug injected}} \times 100$$

$$DL\% = \frac{\text{wight of drug in nanoparticles}}{\text{weight of nanoparticles taken}} \times 100$$

$$Na_2CO_3\% = \frac{\text{weight of } Na_2CO_3 \text{ in nanoparticles}}{\text{weight of nanoparticles taken}} \times 100$$

Stability of ESNs *in vitro*

The ESNs were redispersed in deionized water and stored at 4 °C for 7 days, during which, samples were removed and analyzed for the particle size and zeta potential everyday, as described in Section 2.3.1.

Release of BBR and EVO from ESNs *in vitro*

The release of BBR and EVO from ESNs was measured using a dynamic dialysis method. Briefly, 5 mg of nanoparticles in 1 mL of deionized water were placed into a dialysis bag with a molecular weight cutoff of 12 000 Da and dialyzed against 100 mL of PBS (pH 5.0, 6.8, 7.4) under gentle shaking at 100 rpm at 37 °C. At each scheduled time point, a 2 mL sample was taken from the release medium and the same volume of PBS was replenished accordingly. The samples were assayed for drug content using HPLC. Each experiment was conducted in triplicate.

Disintegration of ESNs *in vitro*

ESNs were redispersed in three PBS solutions of pH values at 5.0, 6.8 and 7.4. After 1, 4, 7 or 14 days of incubation, the samples were dried under vacuum for 24 hours. The disintegration process of the nanocarriers under different pH value conditions were monitored by TEM analysis.[17]

Cytotoxicity of ESNs *in vitro*

MCF-7 cells, HEK-293 cells and HUVECs were cultured in 96-well plates (5×10^3 cells per well), and exposed to different concentrations of nanoparticles for 36 h at 37 °C. Then, the cell viability was assayed using the MTT assay, and each concentration was tested in six wells. Three independent experiments were performed.

Wound-healing assay

The effects of ESNs on cancer cell migration were measured in a wound healing assay.[21] Briefly, MCF-7 cells were cultured in 6-well plates (2×10^5 cells per well), and the plates were cultured overnight. After the cells had reached 70–80% confluence, the medium was aspirated. A pipet tip of approximately 1 mm wide was then used to scratch the monolayer. Then, fresh DMEM containing drugs (20 μg mL^{-1}) was added, and the plates were incubated for 12 h at 37 °C. Phase-contrast fluorescence microscopy (IX71S1F-3, Olympus Optical, Tokyo, Japan) was used to observe the linear wound in the monolayer at 0 and 12 h, and the experimental results were analyzed with Image J software. Wound closure was calculated by dividing the gap width at 12 h by the gap width at 0 h. Three independent experiments were performed.

Hoechst assay

Tumor cell apoptosis was assayed using a Hoechst Staining Kit and fluorescence microscopy. MCF-7 cells were cultured in 6-well plates (1.5×10^5 cells per well) containing coverslips and incubated overnight. After the cells had reached 70–80% confluence, the medium was aspirated. Fresh DMEM containing drugs (25 μg mL^{-1}) was then added, and the plates were incubated for 12 h at 37 °C. Then, the medium was aspirated, the binding solution was added, and fixation was allowed to proceed for 15 min. Coverslips were washed twice with PBS and manual shaking. Hoechst stain was added and staining was allowed to proceed for 15 min, according to the manufacturer's instructions. Coverslips were washed twice again, and then examined by phase-contrast fluorescence microscopy.

Annexin V-FITC assay

MCF-7 cells were cultured in 6-well plates (1.5×10^5 cells per well) and incubated overnight. After the cells had reached 70–80% confluence, the medium was aspirated. Fresh DMEM containing drugs (25 μg mL^{-1}) was added, and the plates were incubated for 12 h at 37 °C. Floating cells were collected, and adherent cells were collected using trypsin digestion. The two fractions of cells were pooled and centrifuged, and the precipitation was incubated with 200 μL FITC/PI buffer at room temperature on the shaker for 15 min in the dark. Then, the cells were analyzed on a flow cytometer (BD Biosciences, San Jose, CA, USA).

Applicability of ESNs

SiO$_2$–COP–Na$_2$CO$_3$@EVO-LB. Nanoparticles containing the synergistic and hydrophobic drugs, EVO and COP, (data not published) were prepared as described in Section 2.2. The particle size and zeta potential of ESNs-A$_1$ were measured as described in Section 2.3.1. The EE% and DL% of EVO and COP in ESNs-A$_1$ were determined as described in Section 2.3.3. The release of EVO and COP from ESNs-A$_1$ was measured as described in Section 2.5. The cytotoxicity of ESNs-A$_1$ *in vitro* was assayed as described in Section 2.7.

SiO$_2$–LUT–Na$_2$CO$_3$@C3G-LB. Nanoparticles containing the synergistic and hydrophobic drugs, LUT and C3G,[22] were prepared as described in Section 2.2. The particle size and zeta potential of ESNs-A$_2$ were measured as described in Section 2.3.1. The EE% and DL% of C3G and LUT in ESNs-A$_2$ were determined as described in Section 2.3.3. The release of C3G and LUT from ESNs-A$_2$ was measured as described in Section 2.5. The cytotoxicity of ESNs-A$_2$ *in vitro* was assayed as described in Section 2.7.

Statistical analysis

All data were analyzed statistically using SPSS 13.0 (IBM, Chicago, IL, USA). All results were expressed as the mean ± SD. Differences associated with $p < 0.05$ were considered significant.

Results

Preparation and characterization of ESNs

A tetraethyl orthosilicate hydrolysis method was employed to prepare ESNs, which is simple and readily scaled up. Table 1 shows the characterization of SiO$_2$–BBR–Na$_2$CO$_3$ and SiO$_2$–BBR–Na$_2$CO$_3$@EVO-LB (ESNs). The size of ESNs was 294.9 ± 3.9 nm, and the polydispersity index (PDI) was 0.234 ± 0.007. Meanwhile, ESNs had high entrapment efficiency and drug loading. Transmission electron microscope (TEM) photographs showed that the ESNs were spherical in shape with a smooth surface and uniform distribution (Fig. 2A). The size distribution and zeta potential distribution of ESNs are shown in Fig. 2B and C. The elemental mapping was taken from two compositional elements: Si and N (a major compositional element of BBR). As

Table 1 Physical properties of various nanoparticles ($n = 3$)[a]

Nanoparticles	Size (nm)	Polydispersity index	Zeta potential (mV)	Entrapment efficiency (%)		Drug loading (%)	
				BBR	EVO	BBR	EVO
SiO₂–BBR–Na₂CO₃	194.1 ± 1.9	0.093 ± 0.036	-14.5 ± 1.6	20.35 ± 1.36	—	8.14 ± 1.02	—
SiO₂–BBR–Na₂CO₃@EVO-LB	294.9 ± 3.9	0.234 ± 0.007	-24.2 ± 0.6	—	97.80 ± 0.14	—	44.01 ± 0.52

[a] Abbreviation: BBR, berberine; EVO, evodiamine.

shown in Fig. 2D and E, N was found to be more concentrated in the center of the SNs, where Si was comparatively less distributed. In comparison, Si appeared to be present in the peripheral regions of the SNs, where N was relatively less dispersed.

Stability of ESNs *in vitro*

As shown in Fig. 2F, ESNs remained stable for at least 7 days at 4 °C without a significant change in the size and zeta potential. Also, no significant alteration in the physical appearance and particle aggregation was observed. These results indicated that the as-prepared ESNs met the needs of stable nanoparticles for subsequent experiments.

Release of BBR and EVO from ESNs *in vitro*

Release profiles of BBR and EVO from ESNs *in vitro* were measured to assess the release of hydrophobic drugs in response to changes in pH. It can be seen from Fig. 3 that BBR and EVO were released from ESNs in a pH-dependent manner. The release amount of the two drugs gradually increases as the pH value of the release medium decreases. This suggests that the result may be mostly due to the gas generation derived from the reaction between Na_2CO_3 in the nanoparticles and H^+ in the release medium, so as to promote the release of the drugs.

Decomposition of ESNs *in vitro*

In order to investigate the decomposition process of the nano-carriers under different pH value conditions simulating *in vivo* situations, we compared the drug release in phosphate buffered saline (PBS) at 37 °C at three different pH values, *i.e.*, pH ∼ 7.4 (normal physiological conditions), pH ∼ 6.8 (tumor microenvironment conditions), and pH ∼ 5.0 (endosomes/lysosomes of tumor cells), respectively. As shown in Fig. 4, the morphology and size of ESNs remained unchanged in PBS at pH 7.4. Conversely, clear morphological changes in the form of increments in size were observed after 4 days for ESNs in PBS at pH 6.8. The nanoparticles became bigger and bigger, although their shape remained intact. In contrast, from day 4 to day 14, the morphology changed remarkably in PBS at pH = 5.0, with the
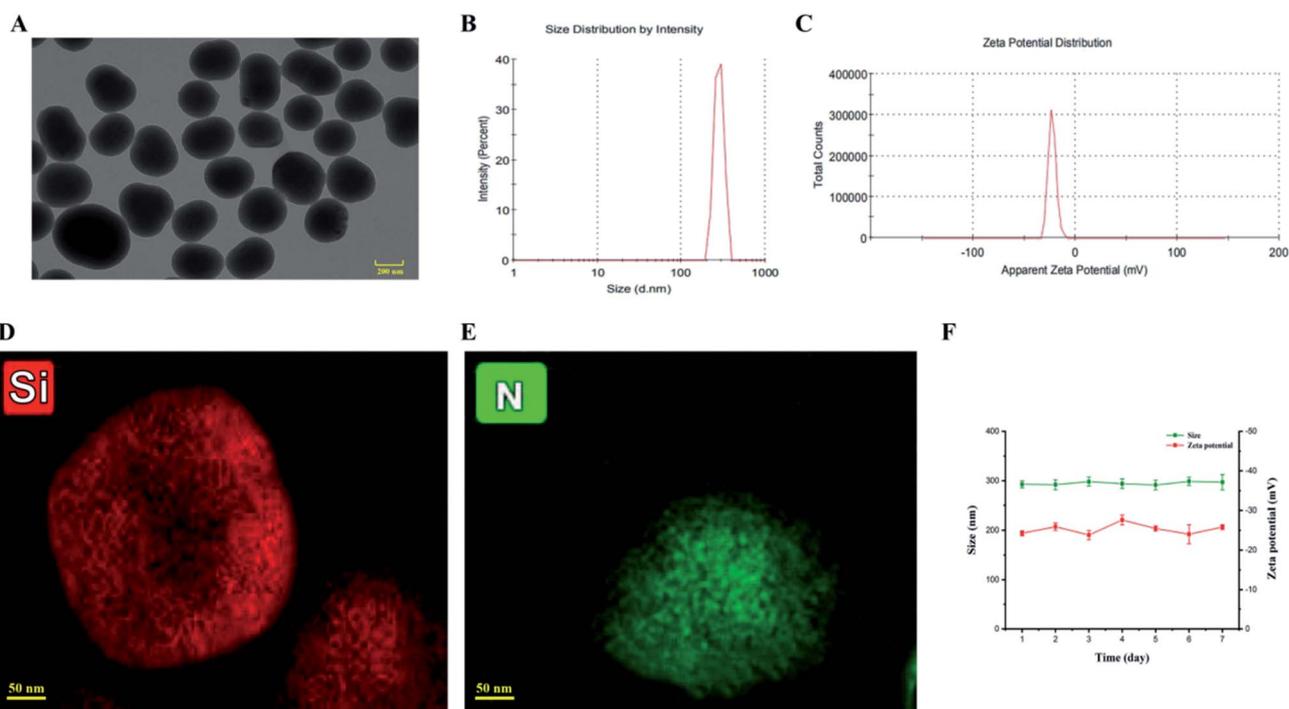

Fig. 2 Characterization and stability of the nanoparticles. Note: TEM photograph of ESNs (A). Size distribution of ESNs (B) and zeta potential distribution of ESNs (C). The elemental mapping of silicon (D) and nitrogen (E). Stability of ESNs (F).
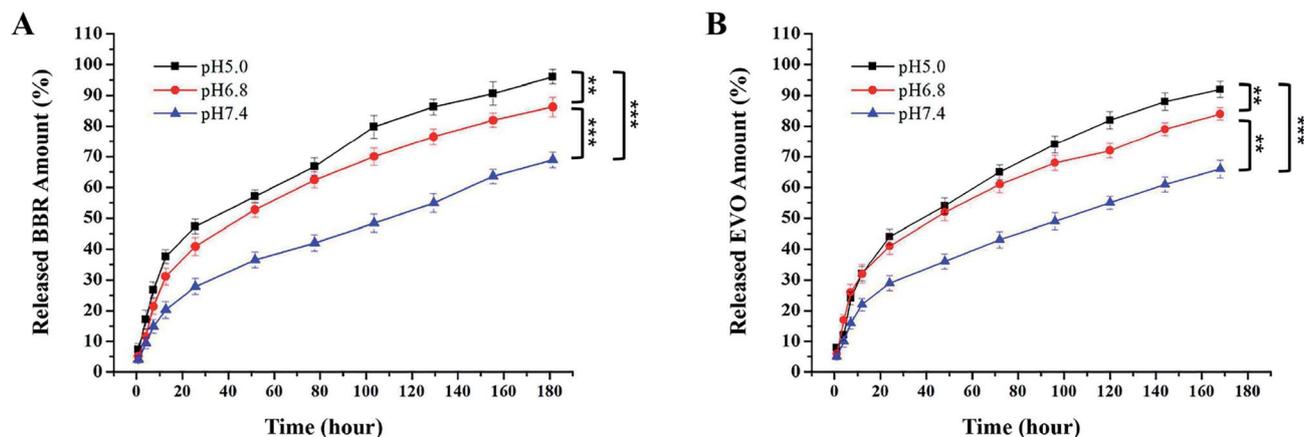
Fig. 3 Release of BBR (A) and EVO (B) from ESNs *in vitro* at different pH values over 168 h ($n = 3$). Note: ** denotes $P < 0.01$, *** denotes $P < 0.001$. Abbreviation: BBR, berberine; EVO, evodiamine.

size becoming larger and larger. In the meantime, the border between the nanocarriers disappeared, and eventually presented as foggy. It is suggested that this is the decomposition of ESNs since the effervescent agent Na_2CO_3 in ESNs reacted with the H^+ in the PBS to generate CO_2, which may promote the disintegration of the nanocarriers.

In vitro cytotoxicity study

To evaluate the biocompatibility of the fabricated nanoparticles, the cytotoxicity of the blank ESNs against HEK-293 cells and HUEVCs was determined under various concentrations. Blank ESNs had no significant influence on the proliferation of HEK-293 cells and HUEVCs up to 100 μg mL^{-1}. The survival rate of HEK-293, as well as HUEVC cells reached 89%

and 82%, respectively (Fig. 5A), which indicated that blank ESNs may be a safe drug carrier.

However, for the breast tumor cells MCF-7, when the blank carrier did not contain Na_2CO_3, the survival rate of the MCF-7 cells was still as high as 83% even the carrier concentration reached 100 μg mL^{-1}. Conversely, for the blank carrier containing Na_2CO_3, the survival rate of MCF-7 cells was significantly reduced (Fig. 5A). This indicated that when the blank carrier contained Na_2CO_3, it had a toxic effect on the MCF-7 cells. This may be due to the fact that when Na_2CO_3 was encapsulated in the carrier after being endocytosed by the tumor cells, a large amount of CO_2 is released in the acidic environment of the tumor cells. This results in damage to the lysosomes of the tumor cells, and thereby leads to cell death.
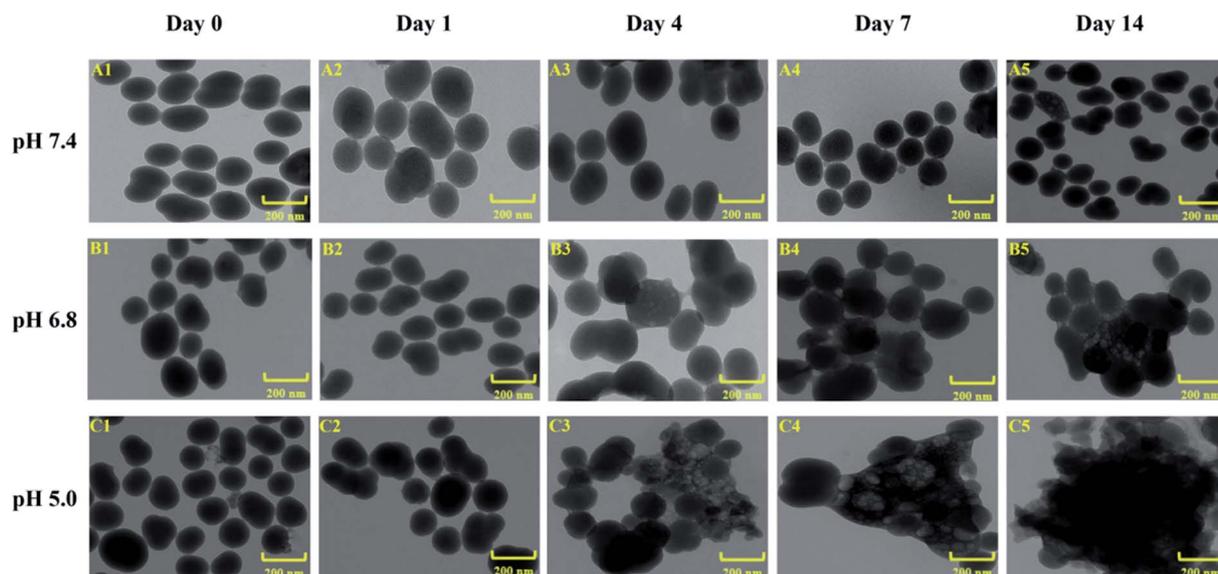

Fig. 4 TEM photographs of ESNs disintegration process *in vitro* under different pH value conditions simulating *in vivo* situations. (A1–A5) The morphology and size of ESNs remained unchanged in PBS at pH 7.4. (B1–B5) Clear morphological changes in the form of increments in size after 4 days for ESNs in PBS at pH 6.8. The nanoparticles became bigger and bigger, but the shape remained intact. (C1–C5) From day 4 to day 14, the morphology changed remarkably in PBS at pH 5.0. The size got larger and larger, and the border between the nanocarriers disappeared.
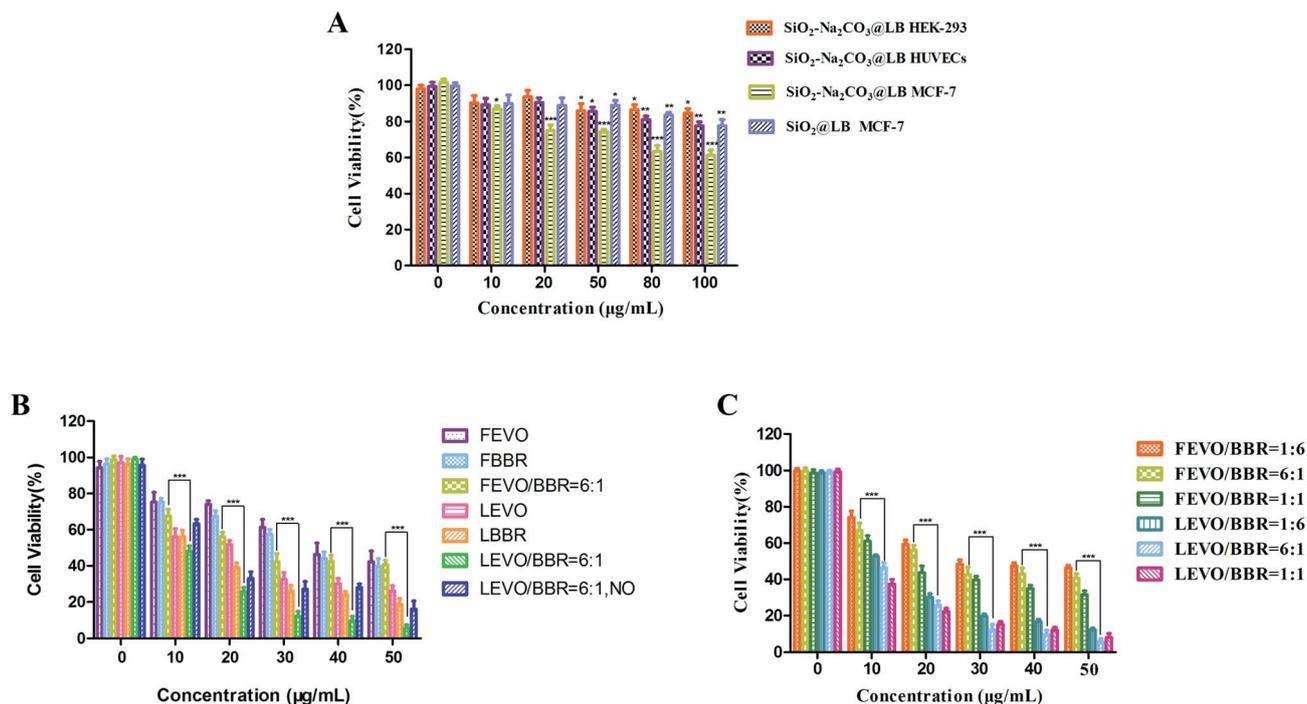
Fig. 5 *In vitro* cytotoxicity analysis of the blank nanoparticles, free BBR/EVO, and BBR/EVO nanoparticles against HEK-293 cells, HUEVCs and MCF-7 cells after 36 h treatment. Notes: Cell viability assay was performed by MTT assay. (A) Cytotoxicity of the blank carrier nanoparticles against HEK-293 cells, HUEVCs and MCF-7 cells. * $P < 0.05$, ** $P < 0.01$, *** $P < 0.001$ *vs.* control group. (B) Cytotoxicity of free BBR/EVO and drug-loaded nanoparticles against MCF-7 cells. *** Denotes $P < 0.001$. (C) Cytotoxicity of different ratios of free BBR/EVO, drug-loaded nanoparticles against MCF-7 cells. *** Denotes $P < 0.001$. Abbreviation: FEVO, free evodiamine; FBBR, free berberine; FEVO/BBR, mechanically mixed free evodiamine and berberine; LEVO, SiO$_2$–Na$_2$CO$_3$@EVO-LB; LBBR, SiO$_2$–BBR–Na$_2$CO$_3$@LB; LEVO/BBR, SiO$_2$–BBR–Na$_2$CO$_3$@EVO-LB; NO, no Na$_2$CO$_3$.

Subsequently, the cytotoxicity of various formulations against MCF-7 cells was examined. The different drug groups refer to our previous research.[23] As shown in Fig. 5B, the drug-loaded nanoparticles had stronger cytotoxicity compared with the free drugs, and achieved a good inhibitory effect on the MCF-7 cells. In addition, the survival rate of the LEVO/BBR (6 : 1) group reached the lowest value at 50 μg mL^{-1}, only 9.61%. Fig. 5C shows the inhibitory effect of the free drugs and drug-loaded nanoparticles with different synergistic ratios on the proliferation of MCF-7 cells, indicating that the synergistic effect of EVO and BBR can be better exerted by the loading of the nanoparticles.

Table 2 shows that the IC$_{50}$ values of different drug groups against the MCF-7 cells and drug-loaded nanoparticles exhibited lower IC$_{50}$ values (3-fold lower than free drugs), which could be caused by the enhanced cellular uptake. Meanwhile, the

drug-loaded nanoparticles containing Na$_2$CO$_3$ showed lower IC$_{50}$ values than the nanoparticles without Na$_2$CO$_3$. It further showed that Na$_2$CO$_3$ exerted an inhibitory effect by itself or in coordination with drugs on tumor cells.

Wound-healing assay

We also studied the effect of established nanoparticles on tumor cell migration and wound-healing. In the results of the wound-healing tests (Fig. 6A), compared with the 0 h group, the control group was associated with 43.87% wound closure; FEVO, 24.63%; FBBR, 36.75%; and FEVO/BBR (6 : 1), 32.19% (Fig. 6B). Much less wound closure was observed with LEVO/BBR (6 : 1, NO) (16.26%) and LEVO/BBR (6 : 1) (12.14%). These results indicate that the loading of hydrophobic drugs into the nanoparticles can better inhibit the invasion and migration of tumor cells, and enhance their synergistic effects.

Table 2 IC$_{50}$ values of different drug groups against MCF-7 cells ($n = 6$)[a]

	IC$_{50}$ (μg mL^{-1})						
Cell lines	FEVO	FBBR	FEVO/BBR = 6 : 1	LEVO	LBBR	LEVO/BBR = 6 : 1, NO	LEVO/BBR = 6 : 1
MCF-7	50.39 ± 1.52	42.03 ± 0.96	31.98 ± 0.88	19.40 ± 0.75	14.81 ± 1.16	16.01 ± 1.27	10.18 ± 0.72

[a] Abbreviation: IC$_{50}$, half-maximal inhibitory concentration; FEVO, free evodiamine; FBBR, free berberine; FEVO/BBR, mechanically mixed free evodiamine and berberine; LEVO, SiO$_2$–Na$_2$CO$_3$@EVO-LB; LBBR, SiO$_2$–BBR–Na$_2$CO$_3$@LB; LEVO/BBR, SiO$_2$–BBR–Na$_2$CO$_3$@EVO-LB; NO, no Na$_2$CO$_3$.

A

Wound Healing
12 h

0 h | Control | FEVO | FBBR | FEVO/BBR (6:1) | LEVO/BBR (6:1), NO | LEVO/BBR (6:1)
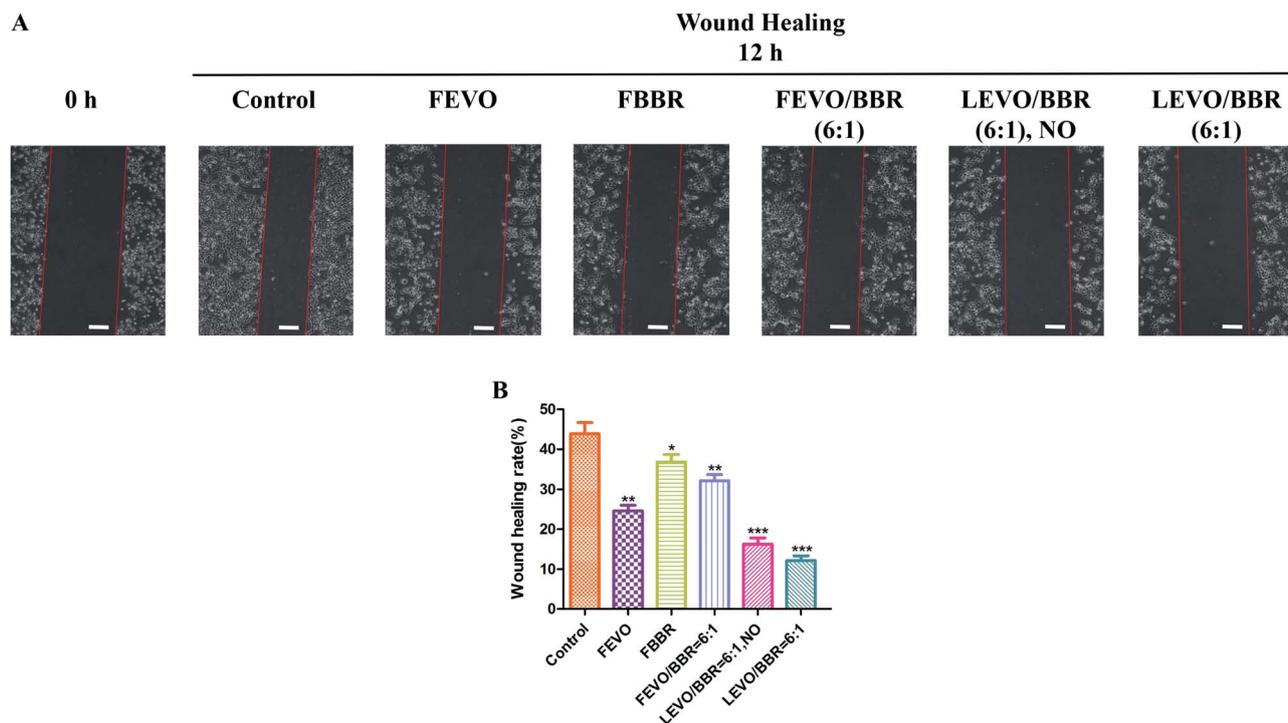
B

Fig. 6 Typical micrographs of wound healing (A). Quantification of wound healing (B) at 12 h after scratching, and treatment with different drugs at 20 μg mL^{-1}. Scale bar, 50 μm. Note: * $P < 0.05$, ** $P < 0.01$, *** $P < 0.001$ *vs.* control group. Abbreviation: FEVO, free evodiamine; FBBR, free berberine; FEVO/BBR, mechanically mixed free evodiamine and berberine; LEVO/BBR, SiO$_2$–BBR–Na$_2$CO$_3$@EVO-LB; NO, no Na$_2$CO$_3$.

Cell apoptosis assay

Cell apoptosis is a programmed cell death.[24] In order to confirm the cause of cell death induced by our different groups, we treated MCF-7 cells with FEVO, FBBR, FEVO/BBR (6 : 1), LEVO/BBR (6 : 1, NO), and LEVO/BBR (6 : 1) for 12 h, and then analyzed the nuclear morphology using fluorescence microscopy (Fig. 7). Compared with the control group, the cells treated with drugs showed chromatin condensation, as well as nuclear fragmentation and shrinkage, indicating apoptosis. Meanwhile, the number of dead cells and the degree of apoptotic chromatin condensation were greater in the cells treated with the drug-loaded nanoparticles than in cells treated with the free drug.

In order to determine the types of apoptotic cell death induced by our different groups, we further analyzed the extent of apoptosis and necrosis using flow cytometry (Fig. 8A). Treating MCF-7 cells with different groups influenced the levels of apoptosis and necrosis, with the percentage of apoptotic cells as follows: FEVO, 18.38%; FBBR, 24.91%; and FEVO/BBR (6 : 1), 26.73%. The higher percentage of apoptosis was observed with LEVO/BBR (6 : 1, NO) (57.38%) and LEVO/BBR (6 : 1) (69.43%). It showed that Na$_2$CO$_3$-containing nanoparticles dual-loaded with EVO and BBR can induce the early apoptosis of tumor cells to the greatest extent and the highest apoptosis rate (Fig. 8B). Meanwhile, compared with the LEVO/BBR (6 : 1, NO) group, the LEVO/BBR (6 : 1) group had a higher percentage of apoptosis, indicating that Na$_2$CO$_3$ may have a certain ability to induce the early apoptosis of tumor cells.

Applicability of ESNs

The experimental results suggest a most attractive and promising NPs carrier-drug system for diagnostic and therapeutic applications. We also attempted to determine whether such simple growth mechanism could be applied to many other molecules employing the SiO$_2$ NP carrier, with the same feature achieved. So, we incorporated other different hydrophobic drug molecules, *i.e.*, COP-EVO, as well as LUT-C3G, into the SiO$_2$ NPs. We then further characterized and determined the inhibitory effects of these different SiO$_2$–drug–Na$_2$CO$_3$ composite nanoparticles.

SiO$_2$–COP–Na$_2$CO$_3$@EVO-LB. Table 3 shows the characterization of SiO$_2$–COP–Na$_2$CO$_3$ and SiO$_2$–COP–Na$_2$CO$_3$@EVO-LB (ESNs-A$_1$). The size was 317.9 ± 1.9 nm and the polydispersity index (PDI) was 0.193 ± 0.007. Meanwhile, ESNs-A$_1$ had a high entrapment efficiency and drug loading. As shown in Fig. 9A and B, COP and EVO were released from ESNs-A$_1$ in a pH-dependent manner similar to SiO$_2$–BBR–Na$_2$CO$_3$@EVO-LB. In addition, the drug-loaded nanoparticles had stronger cytotoxicity against MCF-7 cells than the free drugs (Fig. 9E) in a concentration-dependent mode.

SiO$_2$–LUT–Na$_2$CO$_3$@C3G-LB. Table 4 shows the characterization of SiO$_2$–LUT–Na$_2$CO$_3$ and SiO$_2$–LUT–Na$_2$CO$_3$@C3G-LB (ESNs-A$_2$). The size was 308.9 ± 3.5 nm and the polydispersity index (PDI) was 0.263 ± 0.023. Similarly, ESNs-A$_2$ had a high entrapment efficiency and drug loading. As shown in Fig. 9C and D, the release amount of LUT and C3G gradually increased as the pH value of the release medium decreased. In addition,
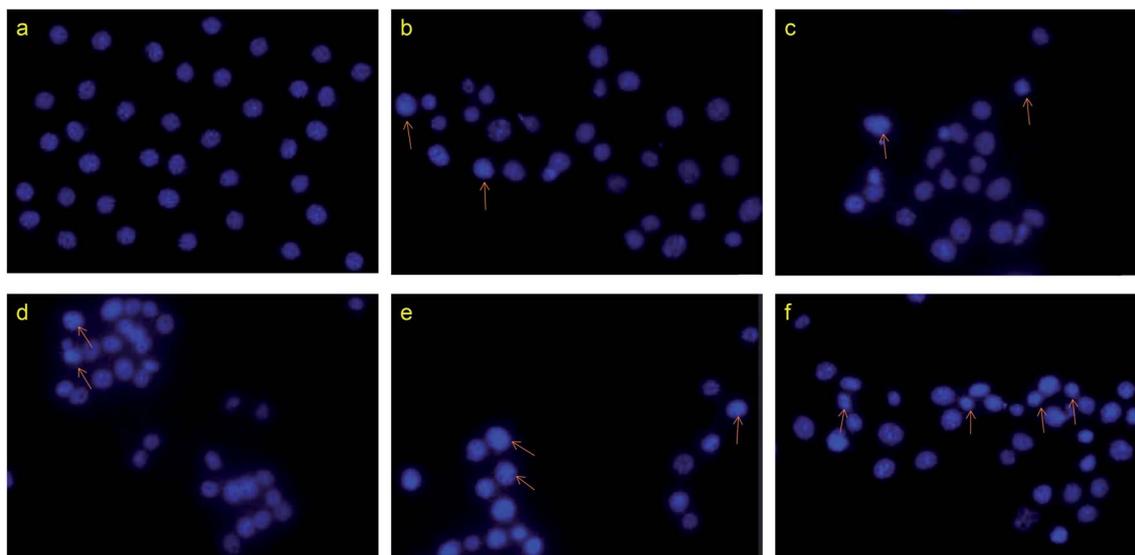
Fig. 7 Fluorescence micrographs of MCF-7 after 12 h incubation with different drugs at 25 µg mL^{-1} and staining with Hoechst 33342. Cell nuclei appear blue. The arrows point to the representative cell chromatin condensation, as well as nuclear fragmentation and shrinkage. Original magnification, 40×. Note: (a) control group; (b) FEVO group; (c) FBBR group; (d) FEVO/BBR (6 : 1) group; (e) LEVO/BBR (6 : 1, NO) group; (f) LEVO/BBR (6 : 1) group. Abbreviation: FEVO, free evodiamine; FBBR, free berberine; FEVO/BBR, mechanically mixed free evodiamine and berberine; LEVO/BBR, SiO$_2$−BBR−Na$_2$CO$_3$@EVO-LB; NO, no Na$_2$CO$_3$.

the drug-loaded nanoparticles achieved an excellent inhibitory effect on the MCF-7 cells compared with the free drugs (Fig. 9F) in a concentration-dependent manner.

These results confirm that ESNs, as a new type of nano-carrier, have a wide range of applications, can load a variety of drugs, especially hydrophobic drugs, and can achieve the ideal antitumor effect. Therefore, ESNs may be a promising dual drug-loaded nano delivery system to improve the antitumor effect of hydrophobic drugs.

Discussion

The effervescent SiO$_2$−drug−Na$_2$CO$_3$ composite nanoparticles constructed in this study added an alkali source (Na$_2$CO$_3$) in
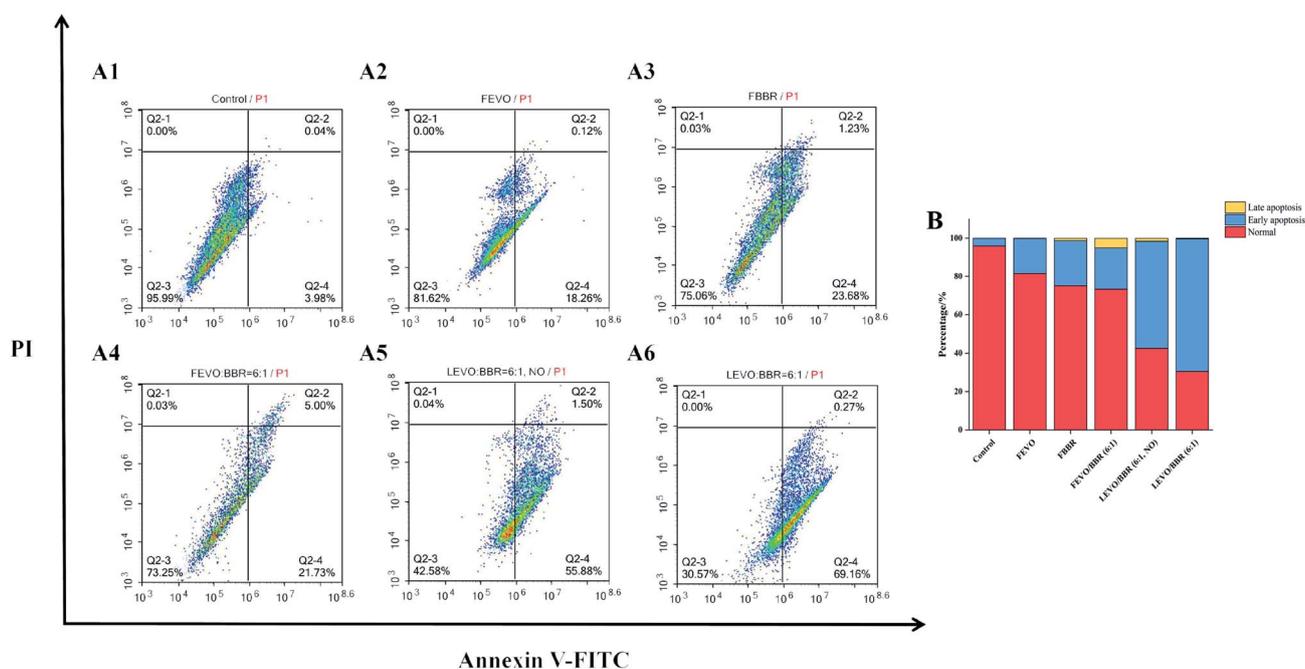

Fig. 8 (A) Analysis of apoptotic stages of MCF-7 cells after 12 h treatment with different drugs at 25 µg mL^{-1}. (B) Statistical analysis data graph. Abbreviation: FEVO, free evodiamine; FBBR, free berberine; FEVO/BBR, mechanically mixed free evodiamine and berberine; LEVO/BBR, SiO$_2$−BBR−Na$_2$CO$_3$@EVO-LB; NO, no Na$_2$CO$_3$.

Table 3 Characterization of various nanoparticles ($n = 3$)[a]

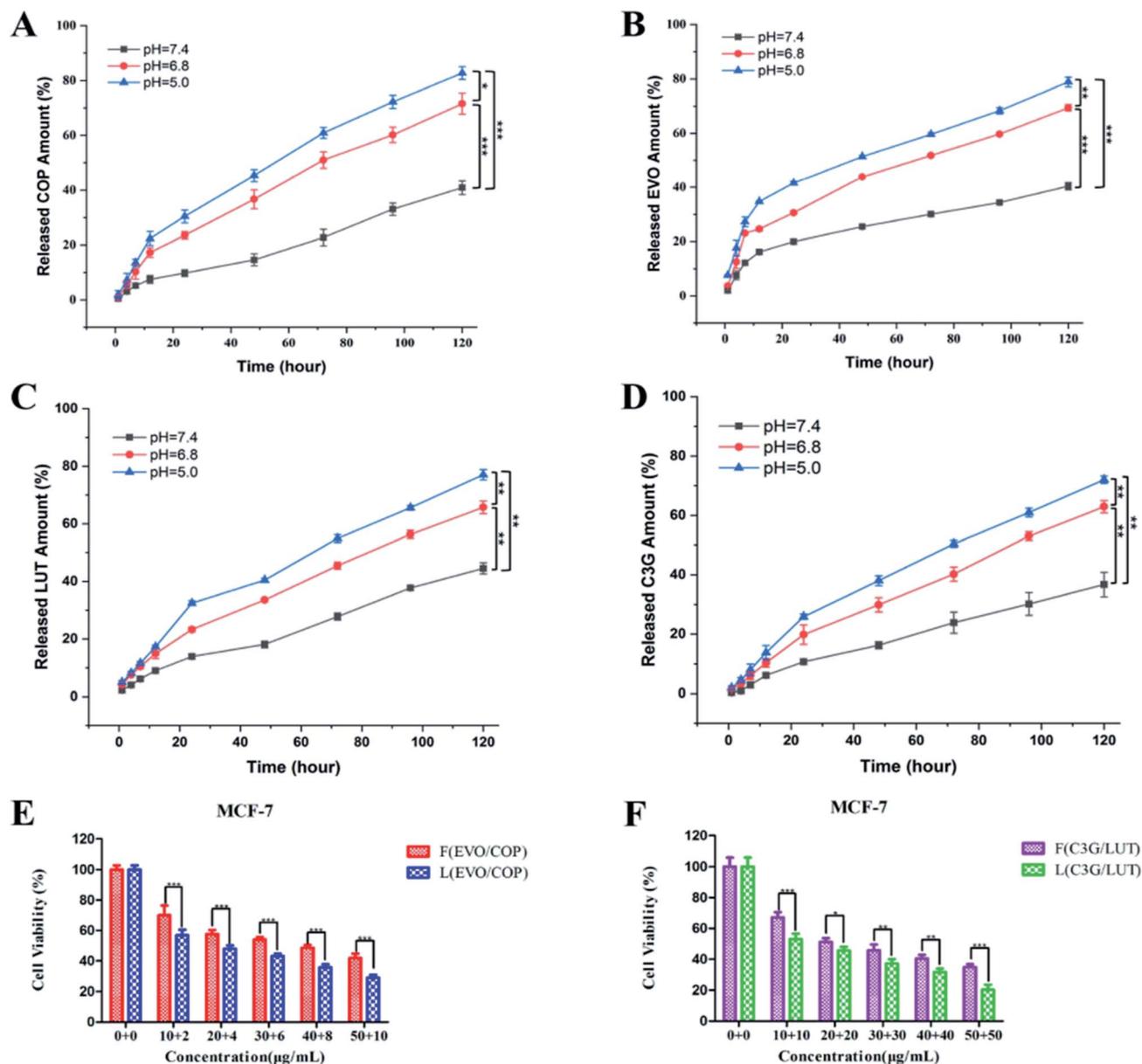| Nanoparticles	Size (nm)	Polydispersity index	Zeta potential (mV)	Entrapment efficiency (%) COP	EVO	Drug loading (%) COP	EVO
SiO$_2$–COP–Na$_2$CO$_3$	205.6 ± 2.8	0.098 ± 0.005	−14.8 ± 1.6	23.69 ± 1.21	—	5.07 ± 0.56	—
SiO$_2$–COP–Na$_2$CO$_3$@EVO-LB	317.5 ± 1.9	0.193 ± 0.007	−27.2 ± 2.1	—	94.75 ± 0.23	—	37.57 ± 1.38

[a] Abbreviation: COP, coptisine; EVO, evodiamine.

Fig. 9 Applicability of nanocarriers. Release of COP (A), EVO (B) LUT (C), and C3G (D) from ESNs *in vitro* at different pH values during 120 h ($n =$ 3). Cell viability assay (E and F) was performed by MTT assay. Note: * $P < 0.05$, ** $P < 0.01$, *** $P < 0.001$. Abbreviation: COP, coptisine; EVO, evodiamine; LUT, luteolin; C3G, cyanidin-3-*O*-glucoside; F(EVO/COP), mechanically mixed free evodiamine and coptisine; L(EVO/COP), SiO$_2$–COP–Na$_2$CO$_3$@EVO-LB; F(C3G/LUT), mechanically mixed free cyanidin-3-*O*-glucoside and luteolin; L(C3G/LUT), SiO$_2$–LUT–Na$_2$CO$_3$@C3G-LB.

Table 4 Physical properties of different nanoparticles ($n = 3$)[a]

Nanoparticles	Size (nm)	Polydispersity index	Zeta potential (mV)	Entrapment efficiency (%)		Drug loading (%)	
				LUT	C3G	LUT	C3G
SiO_2–LUT–Na_2CO_3	198 ± 4.5	0.106 ± 0.015	-16.8 ± 1.1	63.41 ± 2.59	—	25.09 ± 1.67	—
SiO_2–LUT–Na_2CO_3@C3G-LB	308.9 ± 3.5	0.263 ± 0.023	-27.0 ± 0.7	—	41.22 ± 1.51	—	20.53 ± 1.44

[a] Abbreviation: LUT, luteolin; C3G, cyanidin-3-O-glucoside.

Table 5 The notation in this paper

Abbreviation	Full name
BBR	Berberine
C3G	Cyanidin-3-O-glucoside
COP	Coptisine
ESNs	SiO_2–BBR–Na_2CO_3@EVO-LB
ESNs-A1	SiO_2–COP–Na_2CO_3@EVO-LB
ESNs-A2	SiO_2–LUT–Na_2CO_3@C3G-LB
EVO	Evodiamine
LUT	Luteolin

response to the acidic microenvironment of tumor cells, triggering a reaction between the base and H^+ that resulted in the production of large amounts of CO_2. This design accelerated the disintegration of nanoparticles and the release of drugs, significantly improving the anti-tumor effect. The model system of SiO_2–BBR–Na_2CO_3@EVO-LB NPs is a comparatively simple example due to the opposite charge between the alkalized BBR and the silica species. By establishing a radial drug concentration gradient in the nanocarrier, the pH-triggered controllable release of the drug and simultaneous carrier decomposition of the nanoparticles are primarily driven by CO_2 gas generation. A similar procedure was performed for COP-EVO and LUT-C3G, and the results proved successful. In the same way, the present methodology can be universally applied to a vast scope of chemical molecules, and opens a new train of thought for hydrophobic nanodrug design.

In this study, Na_2CO_3 was adopted as an effervescent agent for the production of CO_2 gas, and as an alkalization substrate of quaternary ammonium drugs to improve suppressive activities. It also served as an alkalization agent of the tumor microenvironment, as well as a thermogenic substance originating from dissolution heat for the promotion of drug release and spontaneous carrier decomposition. In addition, Na_2CO_3 dissolution itself may help to boost the drug escape and simultaneous carrier collapse.[25,26] Moreover, Na_2CO_3 manifests considerable anti-tumor effects against a variety of cancer cells, as well as in the present study and other literature.[27–29]

A coating of DSPE-PEG2000 reduces the uptake by macrophages of the mononuclear phagocyte system (MPS), and provides relatively long plasma residence times.[30,31] Meanwhile, SNs modified with a lipid bilayer membrane can achieve the simultaneous loading of two hydrophobic drugs, which can exert the synergistic antitumor effect of the two drugs. The dual drug-loaded nano delivery system with effervescent decomposition qualities induced synergistic effects, leading to higher therapeutic efficacy and target selectivity than the free drugs.

The existing research studies on silica nanoparticles have made great progress in improving the drug loading efficiency and decomposition of carriers in cancer therapeutics.[7,8] However, the methodology can only be applied to hydrophilic drugs.[5,17] The current study has been successful in the loadings of a variety of hydrophobic drugs through the construction of a composite nanosystem (ESNs) with a core–shell structure. ESNs enable the pH-triggered, controllable and comparatively complete release of the hydrophobic drugs and simultaneous carrier decomposition. Nevertheless, in view of the complicated internal environment of the body, the *in vivo* experiments of ESNs should be further conducted (Table 5).

Conclusion

In this study, a lipid membrane-encapsulated, pH-triggered drug release and simultaneous carrier decomposition of effervescent SiO_2–drug–Na_2CO_3 composite nanoparticles was successfully constructed. The results suggest that the disintegration and drug release of the ESNs could be related to the addition of Na_2CO_3, *i.e.*, the base source of effervescent agents reacting with H^+. On the other hand, Na_2CO_3 present in ESNs also function as inhibitors for the suppression of tumor cell proliferation and migration *in vitro via* the mechanism, such as induction cell apoptosis. In conclusion, this novel nanocarrier represents a promising drug delivery system to improve the antitumor effects of synergistic hydrophobic drugs so that the present methodology can be generally applied to a wide scope of chemical molecules, and opens a hopeful vista for the design of a hydrophobic nanodrug.

Conflicts of interest

There are no conflicts to declare.

Acknowledgements

References

1 G. He, Y. Ma, H. Zhou, *et al.* Mesoporous NiS$_2$ nanospheres as a hydrophobic anticancer drug delivery vehicle for synergistic photothermal-chemotherapy, *J. Mater. Chem. B*, 2019, **7**(1), 143–149.

2 K. Dong, Y. Zhang, L. Zhang, Z. Wang, J. Ren and X. Qu, Facile preparation of metal-organic frameworks-based hydrophobic anticancer drug delivery nanoplatform for targeted and enhanced cancer treatment, *Talanta*, 2019, **194**, 703–708.

3 P. Couleaud, V. Morosini, C. Frochot, S. Richeter, L. Raehm and J.-O. Durand, Silica-based nanoparticles for photodynamic therapy applications, *Nanoscale*, 2010, **2**(7), 1083–1095.

4 H. J. Hah, G. Kim, Y.-E. K. Lee, *et al.* Methylene Blue-Conjugated Hydrogel Nanoparticles and Tumor-Cell Targeted Photodynamic Therapy, *Macromol. Biosci.*, 2011, **11**(1), 90–99.

5 S. Zhang, Z. Chu, C. Yin, C. Zhang, G. Lin and Q. Li, Controllable drug release and simultaneously carrier decomposition of SiO$_2$-drug composite nanoparticles, *J. Am. Chem. Soc.*, 2013, **135**(15), 5709–5716.

6 N. Pettinelli, S. Rodriguez-Llamazares, Y. Farrag, *et al.* Poly(hydroxybutyrate-co-hydroxyvalerate) microparticles embedded in kappa-carrageenan/locust bean gum hydrogel as a dual drug delivery carrier, *Int. J. Biol. Macromol.*, 2020, **146**, 110–118.

7 F. Catalano and P. P. Pompa, Design Rules for Mesoporous Silica toward the Nanosize: A Systematic Study, *ACS Appl. Mater. Interfaces*, 2019, **11**(50), 47237–47246.

8 X. Li, G. He, H. Jin, *et al.* Dual-Therapeutics-Loaded Mesoporous Silica Nanoparticles Applied for Breast Tumor Therapy, *ACS Appl. Mater. Interfaces*, 2019, **11**(50), 46497–46503.

9 M. Santha Moorthy, S. Bharathiraja, P. Manivasagan, K. D. Lee and J. Oh, Synthesis of surface capped mesoporous silica nanoparticles for pH-stimuli responsive drug delivery applications, *Medchemcomm*, 2017, **8**(9), 1797–1805.

10 R. M. Sabio, A. B. Meneguin, T. C. Ribeiro, R. R. Silva and M. Chorilli, New insights towards mesoporous silica nanoparticles as a technological platform for chemotherapeutic drugs delivery, *Int. J. Pharm.*, 2019, **564**, 379–409.

11 H. Tan, L. Ma, T. Guo, *et al.* A novel fluorescence aptasensor based on mesoporous silica nanoparticles for selective and sensitive detection of aflatoxin B1, *Anal. Chim. Acta*, 2019, **1068**, 87–95.

12 Y. Wu, Z. Xu, W. Sun, *et al.* Co-responsive smart cyclodextrin-gated mesoporous silica nanoparticles with ligand-receptor engagement for anti-cancer treatment, *Mater. Sci. Eng., C*, 2019, **103**, 109831.

13 Q. Yan, X. Guo, X. Huang, *et al.* Gated Mesoporous Silica Nanocarriers for Hypoxia-Responsive Cargo Release, *ACS Appl. Mater. Interfaces*, 2019, **11**(27), 24377–24385.

14 S. Khatoon, H. S. Han, J. Jeon, *et al.* Hypoxia-Responsive Mesoporous Nanoparticles for Doxorubicin Delivery, *Polymers*, 2018, **10**(4), 390.

15 N. V. Rao, H. S. Han, H. Lee, *et al.* ROS-responsive mesoporous silica nanoparticles for MR imaging-guided photodynamically maneuvered chemotherapy, *Nanoscale*, 2018, **10**(20), 9616–9627.

16 D. Sen Karaman, G. Patrignani, E. Rosqvist, *et al.* Mesoporous silica nanoparticles facilitating the dissolution of poorly soluble drugs in orodispersible films, *Eur. J. Pharm. Sci.*, 2018, **122**, 152–159.

17 A. Li, J. Zhang, Y. Xu, J. Liu and S. Feng, Thermoresponsive copolymer/SiO2 nanoparticles with dual functions of thermally controlled drug release and simultaneous carrier decomposition, *Chemistry*, 2014, **20**(40), 12945–12953.

18 H. Wu, L. Zhu and V. P. Torchilin, pH-sensitive poly(histidine)-PEG/DSPE-PEG co-polymer micelles for cytosolic drug delivery, *Biomaterials*, 2013, **34**(4), 1213–1222.

19 X. Ji, W. Zhang, L. Shan, Y. Tian and J. Liu, Self-assembly preparation of SiO2@Ni-Al layered double hydroxide composites and their enhanced electrorheological characteristics, *Sci. Rep.*, 2015, **5**, 18367.

20 N. Li, Y. Chen, H. Sun, *et al.* Decreasing acute toxicity and suppressing colorectal carcinoma using Sorafenib-loaded nanoparticles, *Pharm. Dev. Technol.*, 2020, **25**(5), 556–565.

21 C.-C. Liang, A. Y. Park and J.-L. Guan, In vitro scratch assay: a convenient and inexpensive method for analysis of cell migration in vitro, *Nat. Protoc.*, 2007, **2**(2), 329–333.

22 H. Yin, L. Wang, M. Wu, Y. Liu, N. Li and T. Chen, Cyanidin-3-O-glucoside chloride acts synergistically with luteolin to inhibit the growth of colon and breast carcinoma cells, *Pharmazie*, 2019, **74**(1), 54–61.

23 Y. Feng, N. X. Li, H. L. Yin, T. Y. Chen, Q. Yang and M. Wu, Thermo- and pH-responsive, Lipid-coated, Mesoporous Silica Nanoparticle-based Dual Drug Delivery System To Improve the Antitumor Effect of Hydrophobic Drugs, *Mol. Pharm.*, 2019, **16**(1), 422–436.

24 M. Shi, J. Zhang, X. Li, *et al.* Mitochondria-targeted delivery of doxorubicin to enhance antitumor activity with HER-2 peptide-mediated multifunctional pH-sensitive DQAsomes, *Int. J. Nanomed.*, 2018, **13**, 4209–4226.

25 K.-J. Chen, E.-Y. Chaung, S.-P. Wey, *et al.* Hyperthermia-Mediated Local Drug Delivery by a Bubble-Generating Liposomal System for Tumor-Specific Chemotherapy, *ACS Nano*, 2014, **8**(5), 5105–5115.

26 Z. Deng, M. Tang, L. Zhao, *et al.* Targeted H+-Triggered Bubble-Generating Nanosystems for Effective Therapy in Cancer Cells, *Colloids Surf., B*, 2017, **160**, 207–214.

27 Z. Wen, Y. Long, L. Yang, *et al.* Constructing H+-triggered bubble generating nano-drug delivery systems using bicarbonate and carbonate, *RSC Adv.*, 2016, **6**(107), 105814–105820.

28 L. Yang, Z. Wen, Y. Long, *et al.* A H+-triggered bubble-generating nanosystem for killing cancer cells, *Chem. Commun.*, 2016, **52**(72), 10838–10841.

Paper

29 M. Gautam, R. K. Thapa, B. K. Poudel, *et al.* Aerosol technique-based carbon-encapsulated hollow mesoporous silica nanoparticles for synergistic chemo-photothermal therapy, *Acta Biomater.*, 2019, **88**, 448–461.

30 B. Romberg, W. E. Hennink and G. Storm, Sheddable coatings for long-circulating nanoparticles, *Pharm. Res.*, 2008, **25**(1), 55–71.

31 D. Wang, Y. Wang, G. Zhao, J. Zhuang and W. Wu, Improving systemic circulation of paclitaxel nanocrystals by surface hybridization of DSPE-PEG2000, *Colloids Surf., B*, 2019, **182**, 110337.